Mapping of spatial distribution of superficial blood vessels in human skin by double correlation analysis of Optical Coherence Tomography images

A. Doronin *a, S. Boting a, M. Meglinski b, K. Jentoft and I. Meglinski a

- a Department of Physics, University of Otago, P.O. Box 56, Dunedin, 9054, New Zealand
 b Columba College, 399 Highgate, Private Bag 1911, Dunedin 9010, New Zealand
 c Institute for Biological and Medical Imaging, Helmholtz Center, Munich, Germany
 - **ABSTRACT**

2D/3D spatial distribution of superficial blood vessels in human skin *in vivo* was conducted by double correlation analysis of the swept source Optical Coherence Tomography (OCT) images. An adaptive Wiener filtering technique has been employed to remove background noise and increase the overall quality of the OCT images acquired experimentally. Correlation Mapping and Fourier domain correlation approaches have been subsequently applied to enhance spatial resolution of images of vascular network in human skin. The analysis of images performed on Graphics Processing Units (GPUs) utilizing the recently developed Compute Unified Device Architecture (CUDA) framework.

Keywords: human skin, blood vessels, Optical Coherence Tomography, Wiener filter, image processing, CUDA

1. INTRODUCTION

Nowadays cardiovascular diseases (CVD) are becoming increasingly common amongst westerners, and those which are congenital are affecting about 1 per cent of American births and CVD is estimated at US \$448.5 billion in direct and indirect costs [1]. For the last decade, the broadly researched imaging technique known as Optical Coherence Tomography (OCT) has emerged from both medical and industrial applications [2]. It has achieved vast interest and growth, permitting reasonably wide deviations from its original ophthalmological applications [3] to other medical and biomedical applications, including intracoronary [4] and cardiovascular imaging [5,6]. Doppler OCT, an extension of OCT, was shown to be capable for rheological and flow dynamics studies with micrometer resolution [6-8], two dimensional tomographic mapping of flow velocity and vessels morphology [8-10]. Use of Doppler OCT is highly beneficial for simultaneous imaging of changes in blood flow profiles and morphological images of subcutaneous blood vessels into the full depth of the lumen.

Recently several OCT-based technologies have been proposed to visualize subcutaneous vascular bed distribution in human skin with conjoined assessment of tissues morphology and blood circulation. Speckle variance OCT (svOCT) is based on calculation of the variance of a sequence of structural OCT images by using spatial [11] or temporal [12] analysis of the dynamic speckle pattern generated by moving red blood cells. OMAG utilizes a constant modulation frequency to separate from the backscattering signal the signal associated with the motion of erythrocytes in vascular bed [13]. Correlation mapping OCT (cmOCT) applies two dimensional OCT images for reconstruction of skin blood vessel distribution [14].

In current paper we report a further development of correlation-based OCT approach for non-invasive imaging of subcutaneous blood vessels distribution within a human skin with higher resolution compared to the techniques reported earlier.

2. MATERIALS AND METHODS

The standard swept source OCT (OCM1300SS, Thorlabs, Inc.) has been used to acquire 3D volumes of skin images $(3\times3\times1 \text{ mm})$. The system consists of the swept source engine, imaging module and imaging probe with its articulated probe mount for flexible usage. The laser, contained within the swept source engine, has a central wavelength of 1325

Dynamics and Fluctuations in Biomedical Photonics X, edited by Valery V. Tuchin, Donald D. Duncan, Kirill V. Larin, Martin J. Leahy, Ruikang K. Wang, Proc. of SPIE Vol. 8580, 858002 ⋅ © 2013 SPIE CCC code: 1605-7422/13/\$18 ⋅ doi: 10.1117/12.2002729

Proc. of SPIE Vol. 8580 858002-1

^{*} Correspondence: Department of Physics, University of Otago, P.O. Box 56, Dunedin, 9054, New Zealand E-mail: alexd@physics.otago.ac.nz and/or igor@physics.otago.ac.nz Web: http://www.biophotonics. ac.nz

nm with a bandwidth of ~ 100 nm, scanning rate of 16 kHz, and output power of probing light 12 mW. The system is capable of acquiring 3D volume $1024 \times 1024 \times 512$ pixels containing 1024 images within approximately 40 seconds, with respective axial and lateral resolutions of ~ 13-25 μm . The healthy volunteer's forearm (Antebrachium) was placed under the OCT system imaging probe and 3D images have been obtained.

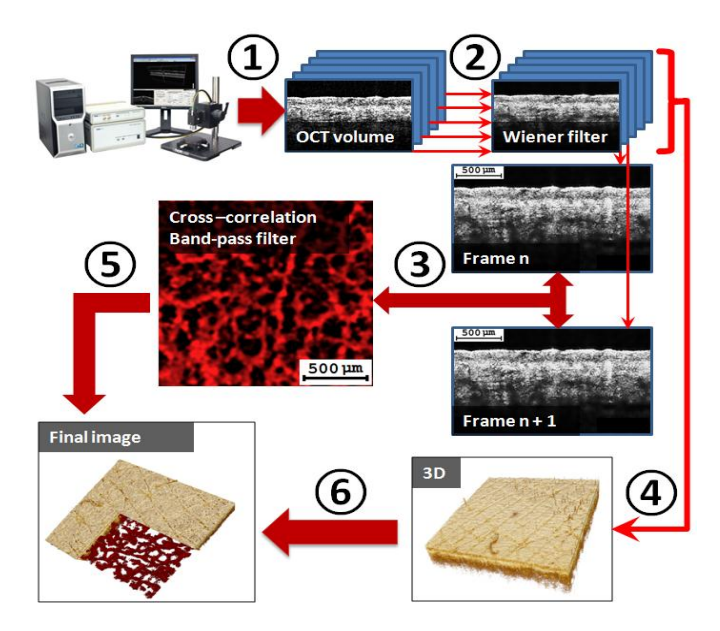


Figure 1. Schematic presentation of principal steps involved in 3D image reconstruction of blood vessels distribution in human skin. Here, step 1 is acquiring a 3D volume of OCT images, step 2 is the Wiener filtering procedure of obtained OCT images, step 3 denotes computing the cross-correlation, step 4 is the generation of a 3D OCT image, step 5 - band-pass filtering to emphasize the regions of interest, step 6 - combining 3D OCT image with the reconstructed blood vessels.

DC works by comparing two OCT images that correspond to the same structural information. Regions of high correlation correspond to structures within the volume which have remained static between the two images, while those of low correlation correspond to motion or flow. The idea is that there is increased contrast between regions of motion, and regions of static structure, so that one is able to map out the vascular blood flow within the volume [14]. Figure 1 schematically represents the main processing steps taken to reconstruct the skin vascular network.

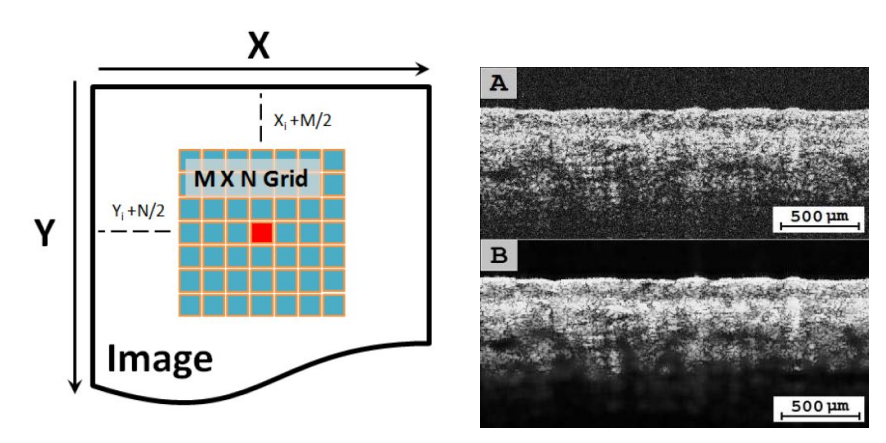


Figure 2. Left: schematic presentation of the Wiener filtering procedure used in this study. A grid M×N pixels is moving along the x-y plane of the image; Right: an example of the OCT image processed by the Wiener filter, where: A - before filtering, B - after filtering (right).

Once a 3D volume of OCT images is acquired, to suppress unwanted background noise, reduce the effects of patient's motions as well as increase the overall quality of the obtained OCT images an adaptive filtering technique known as Wiener filter has been employed. This technique is commonly used in Image Processing and uses a sliding window (or grid) of size of M×N pixels centered on each pixel of the input image (Figure 2, left). Implementation of the optimal Wiener filter W(I) for a grid I requires calculation of the filter's coefficients by obtaining autocorrelations functions (power spectrums) of the OCT signal $P_S(I)$ and noise $P_N(I)$. In the frequency-domain the optimal Wiener filter is obtained as [15]:

$$W(I) = \frac{P_{S}(I)}{P_{S}(I) + P_{N}(I)}$$
 (1)

The additive noise power spectrum was estimated by calculation of the local variance for each grid using two-dimensional correlation [16]. The power spectra of the OCT signal is calculated directly from the image. The desired OCT image signal power spectra for the grid was obtained by subtracting an estimate of the noise spectra from the original OCT images. Finally, all OCT images in the 3D volume were filtered by repeating the same procedure for each pixel. There are other procedures exist (Bayesian implementation of the Wiener filter, hidden Markov models, Additive Noise Reduction, *etc.*) to obtain the autocorrelation functions of signal/noise and are described elsewhere [15]. Figure 2 shows the results of the Wiener filtering of an OCT image.

One of the standard methods to calculate the correlation between two corresponding OCT images is the Correlation Mapping (cmOCT) approach. cmOCT works by comparing a grid I_A from image A(x,y) to the same grid I_B from image B(x,y) defined over x-y plane. The M×N grid is shifted pixel-by-pixel across the images, forming a correlation plane C(x,y) [14]. The output has values in the range -1.0 to 1.0, indicating low correlation to both high positive and high negative correlation. The particular equation used in this study is a simplified version of Normalized Cross-Correlation (NCC):

$$C(x,y) = \sum_{p=0}^{M} \sum_{q=0}^{N} \frac{I_A(p,q)I_B(p,q)}{\sqrt{I_A(p,q)^2 I_B(p,q)^2}},$$
(2)

where

$$I_A(p,q) = I_A(x+p,y+q) - \overline{I}_A,$$

$$I_B(p,q) = I_B(x+p,y+q) - \overline{I}_B.$$

Here, the over bars denote the average values over the grids.

Direct computation of NCC is very computationally expensive and can be optimized by various techniques such as sumtables [16]. Hoverer, a significantly more efficient approach to calculate cross-correlation is based on the Fast Fourier Transform. The Fourier transform is widely used in a large class of signal processing algorithms for fast and efficient function decomposition and analysis [15]. The approach utilizes the Cross-Correlation theorem stating that the Fourier transform of the cross-correlation of two functions is equal to the product of their individual Fourier transforms, where one of them has been complex conjugated. Thus, to find the cross-correlation between two grids the following equation is used:

$$C(x, y) = F^{-1}(F(I_A) \times \overline{F(I_B)}), \tag{3}$$

where

$$F(I_A) = \sum_{x=0}^{M-1} \sum_{y=0}^{N-1} I_A(x, y) e^{-2\pi i (ux/M + vy/N)},$$

$$F(I_B) = \sum_{x=0}^{M-1} \sum_{y=0}^{N-1} I_B(x, y) e^{-2\pi i (ux/M + vy/N)}.$$

Here, $F(I_A)$ is the Fourier Transform of I_A and $\overline{F(I_B)}$ is the complex conjugate of the Fourier Transform $F(I_B)$ of I_A , u and v are spatial frequencies in x and y directions, respectively. The number of frequencies is equal to the number of pixels in the spatial domain image, i.e. both images are of the same size.

For optimized performance, the analysis of the images has been performed on Graphics Processing Units (GPUs) utilizing recently developed Compute Unified Device Architecture (CUDA) framework (Figure 3). CUDA framework

provides access to the CUDA Fast Fourier Transform library (cuFFT). The algorithm allows carrying out FTT computations in parallel utilizing hundreds of GPU cores providing a significant speed up compared to the standard CPU approach (up to $1000 \times \text{faster}$) [17].

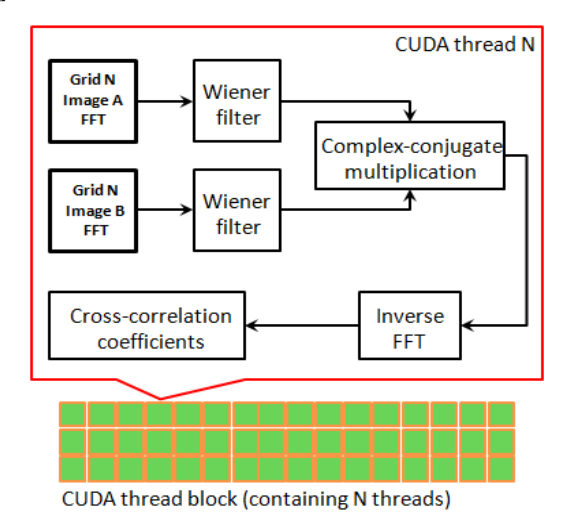


Figure 3. Schematic presentation of the DC performed on GPUs. Each thread processes in parallel the corresponding grids I_A and I_B from images A(x,y) and B(x,y) producing the resulting correlation plane C(x,y).

3. RESULTS AND DISCUSSION

After saving 2D correlation maps into a single directory, a band-pass filter was applied to cutoff frequencies corresponding to the values of the correlation coefficients outside the range -0.4 to 0.4. Band-pass filtering is common technique used for narrowing the range of data without major losses, *i.e.* extracting features of images corresponding to particular structural formations (e.g. blood vessels) [14]. Figure 4, left represents comparison between the two methods for reconstructing the vascular bed, discussed above. In the current study the entire 3D OCT volume $1024 \times 1024 \times 512$ pixels containing 1024 images has been processed on dual Tesla M2090 GPUs within 30 seconds using 7×7 grid. Finally, the OCT images were converted into a 3D mesh, combined with the corresponding reconstruction of the blood vessels and a resulting 3D image has been created (see Figure 4, right).

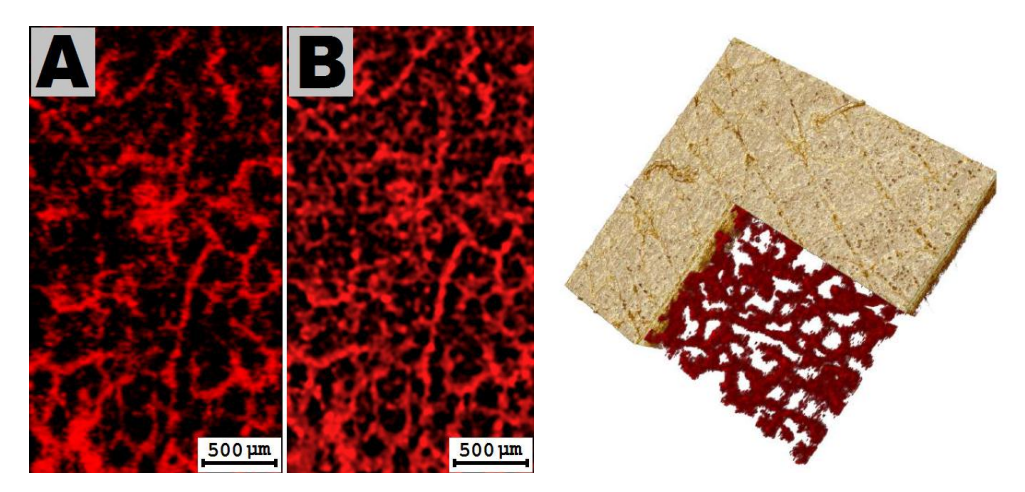


Figure 4. Left: OCT images of superficial blood vessels of human skin *in vivo* corresponding to the depth 550 μm (left), where A - obtained by cmOCT [14], B - obtained by Double Correlation OCT; Right: An example of 3D OCT image of spatial distribution of blood vessels in human skin obtained at 3×3×1 mm scale (right).

4. CONCLUSIONS AND FUTURE WORK

Thus, we demonstrated that the double correlation approach permits obtaining 2D/3D images of superficial blood vessels and their distribution within the human skin with higher resolution compare to the similar techniques reported early. Moreover, Thorlabs, Inc. offers a Software Development Kit (SDK) which allows customers to build custom applications upon. The SDK provides interfaces for OCT Hardware Control, Extensive Processing Routines, Display Options and Data Import/Export. This allows bypassing the step of manual acquisition of the OCT images and provides the opportunity for direct export of the FFT-encoded image data to the processing software. We believe that incorporating this ability in the DC method will significantly improve the quality of the outcomes, speed up the processing and rendering the vascular bed in real-time. Future work will also include a comprehensive study of other implementations of Weiner filter/other image processing approaches including Bayesian implementation, hidden Markov models, Additive Noise Reduction, *etc.* as well as other techniques of optimization of the NCC computing procedure.

5. REFERENCES

- [1] American Heart Association, (2012).
- [2] Tuchin, V. V., [Handbook of Coherent Domain Optical Methods: Biomedical Diagostics, Environment and Material Science], Kluwer Academic, (2004).
- [3] Fercher, A., Drexler, W., Hitzenberger, C., Lasser, T., "Optical coherence tomography principles and applications," Rep. Prog. Phys. 66, 239-303 (2003).
- [4] Lowe, H.C., Narula, J., Fujimoto, J.G., Jang, I.-K., "Intracoronary Optical Diagnostics," J. Am. Coll. Cardiol. Intv. 4(12), 1257-1270 (2011).
- [5] Bonesi, M., Matcher, S., Meglinski, I., "Doppler Optical Coherence Tomography in Cardiovascular Applications," Laser Phys. 20(6), 1491-1499 (2010).
- [6] Bonesi, M., Kennerley, A.J., Meglinski, I., Matcher, S., "Application of Doppler Optical Coherence Tomography in rheological studies: Blood flow and vessels mechanical properties evaluation," Journal of Innovative Optical Health Sciences, 2(4), 431-440 (2009).
- [7] Bonesi, M., Churmakov, D.Y., Ritchie, L.J. Meglinski, I., "Turbulent flow monitoring with Doppler Optical Coherence Tomography," Laser Phys. Let., 4(4), 304-307 (2007).
- [8] Veksler B., Kobzev, E. Bonesi, M., Meglinski, I., "Application of Doppler Optical Coherence Tomography for imaging of scaffold structure and local micro-flow characterization," Laser Phys. Lett., 5(3), 236-239 (2008).
- [9] Bonesi, M., Churmakov, D.Y., Meglinski, I., "Study of flow dynamics in complex vessels by using Doppler Optical Coherence Tomography," Meas. Sci. Technol., 18(11), 3279-3286 (2007).
- [10] Bonesi, M., Proskurin, S., Meglinski, I., "Imaging of subcutaneous blood vessels and flow velocity profiles by Optical Coherence Tomography," Laser Phys., 20(4), 891-899 (2010).
- [11] Barton, J., Stromski, S., "Flow measurement without phase information in optical coherence tomography images," Opt. Express 13(14), 5234-5239 (2005).
- [12] Mariampillai, A., Standish, B.A., Moriyama, E. H., Khurana, M., Munce, N. R., Leung, M. K. K., Jiang, J., Cable, A., Wilson, B. C., Vitkin, I. A., Yang, V. X. D., "Speckle variance detection of microvasculature using swept-source optical coherence tomography", Opt. Lett. 33(13), 1530-1532 (2008).
- [13] Wang, R. K., An, L., Francis, P., Wilson, D. J., "Depth-resolved imaging of capillary networks in retina and choroid using ultrahigh sensitive optical microangiography", Opt. Lett. 35(9), 1467-1469 (2010).
- [14] Jonathan, E., Enfield, J., Leahy, M. J., "Correlation mapping method for generating microcirculation morphology from optical coherence tomography (OCT) intensity images", J. Biophotonics 4(9), 583-587 (2011)
- [15] Gonzalez, R., Woods, R., [Digital Image Processing, 3rd edition], Prentice Hall, (2008).
- [16] Lim, J., [Two-Dimensional Signal and Image Processing], Prentice Hall, (1989).
- [17] Doronin, A.V., Meglinski, I.V., "Online object oriented Monte Carlo computational tool for the needs of biomedical optics," Biomed. Opt. Express, 9, 2461–2469 (2011).

Proc. of SPIE Vol. 8580 858002-5